Carbon Nanotube Microelectrode Arrays Enable Scalable and Accessible Electrophysiological Recordings of Cerebral Organoids

Supplementary Information

Navya Mishra[1], Rajaram Kaveti[1], Pei Liu[2], Baha Erim Uzunoglu[1], Aram Mirabedini[3], Anna Tran[3], Z. Begum Yagci[4], Tyler Johnson[4], Parvez Ahmmed[5], Qiuli Wang[6], Jeong Yong Kim[4], Paris Brown[7], Surjendu Maity[7], Shyni Varghese[7], Michael D. Dickey[4], Yong Zhu[6], Alper Bozkurt[1], Raudel Avila[2], Albert J. Keung[4], Amay J. Bandodkar[1,3]

Authors and Affiliations

1. **Department of Electrical and Computer Engineering, North Carolina State University, Raleigh, NC, USA**
2. **Department of Mechanical Engineering, Rice University, Houston, TX, USA**
3. **Lampe Joint Department of Biomedical Engineering, North Carolina State University, Raleigh and The University of North Carolina, Chapel Hill, NC, USA**
4. **Department of Chemical and Biomolecular Engineering, North Carolina State University, Raleigh, NC, USA**
5. **Advanced Micro Devices (AMD), Inc., Boxborough, MA, USA**
6. **Department of Mechanical and Aerospace Engineering, North Carolina State University, Raleigh, NC, USA**
7. **Department of Biomedical Engineering, Duke University, Durham, NC, USA**

Corresponding authors: Correspondence to Albert J. Keung[4] (ajkeung@ncsu.edu) and Amay J. Bandodkar[1,3] (ajbandod@ncsu.edu)

Table of Contents

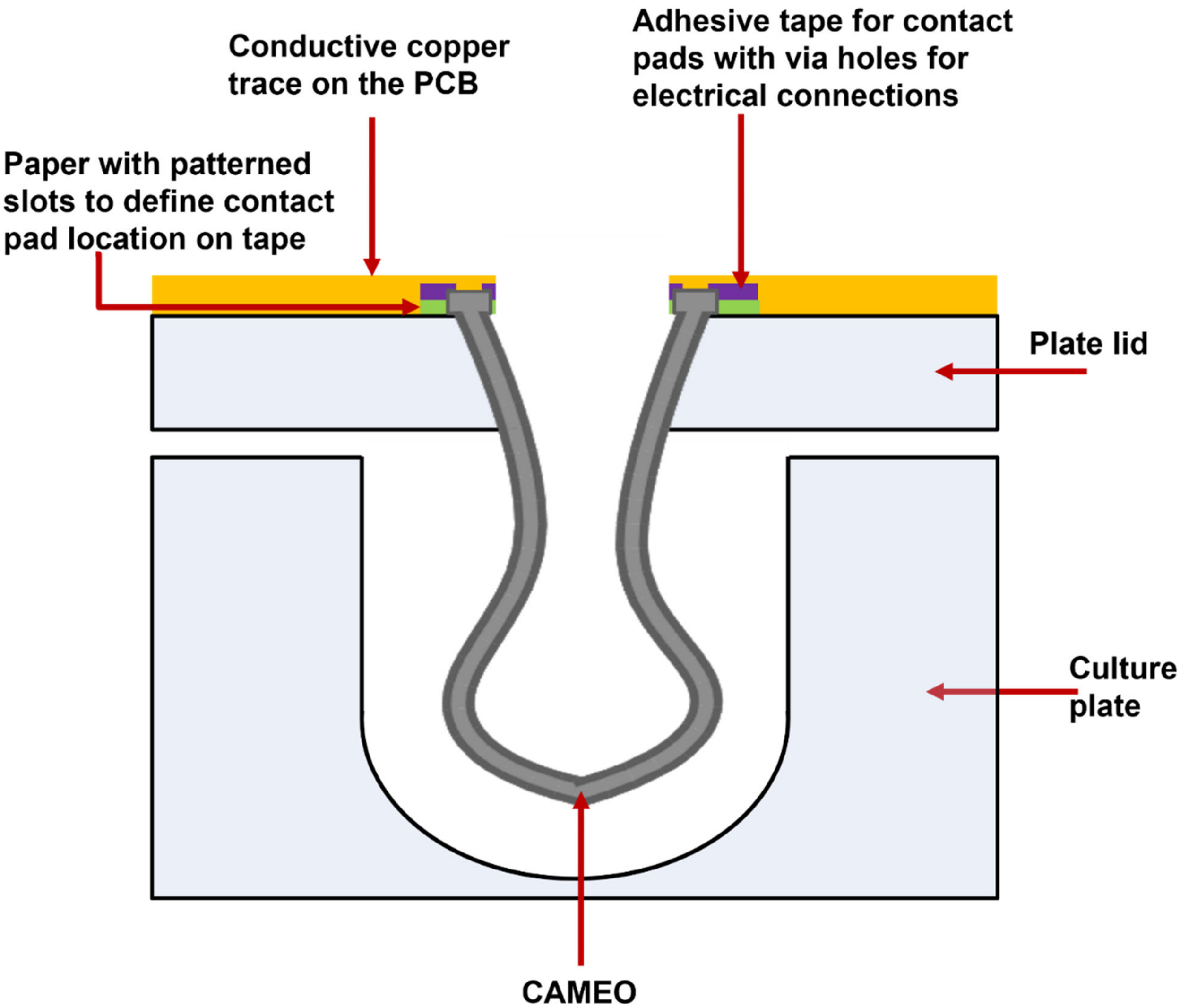

Figure S1: Schematic of the system. Cross section of the system with all key components individually labelled. Partly created in BioRender. Mishra, N. (2026) https://BioRender.com/xvo3sgs.

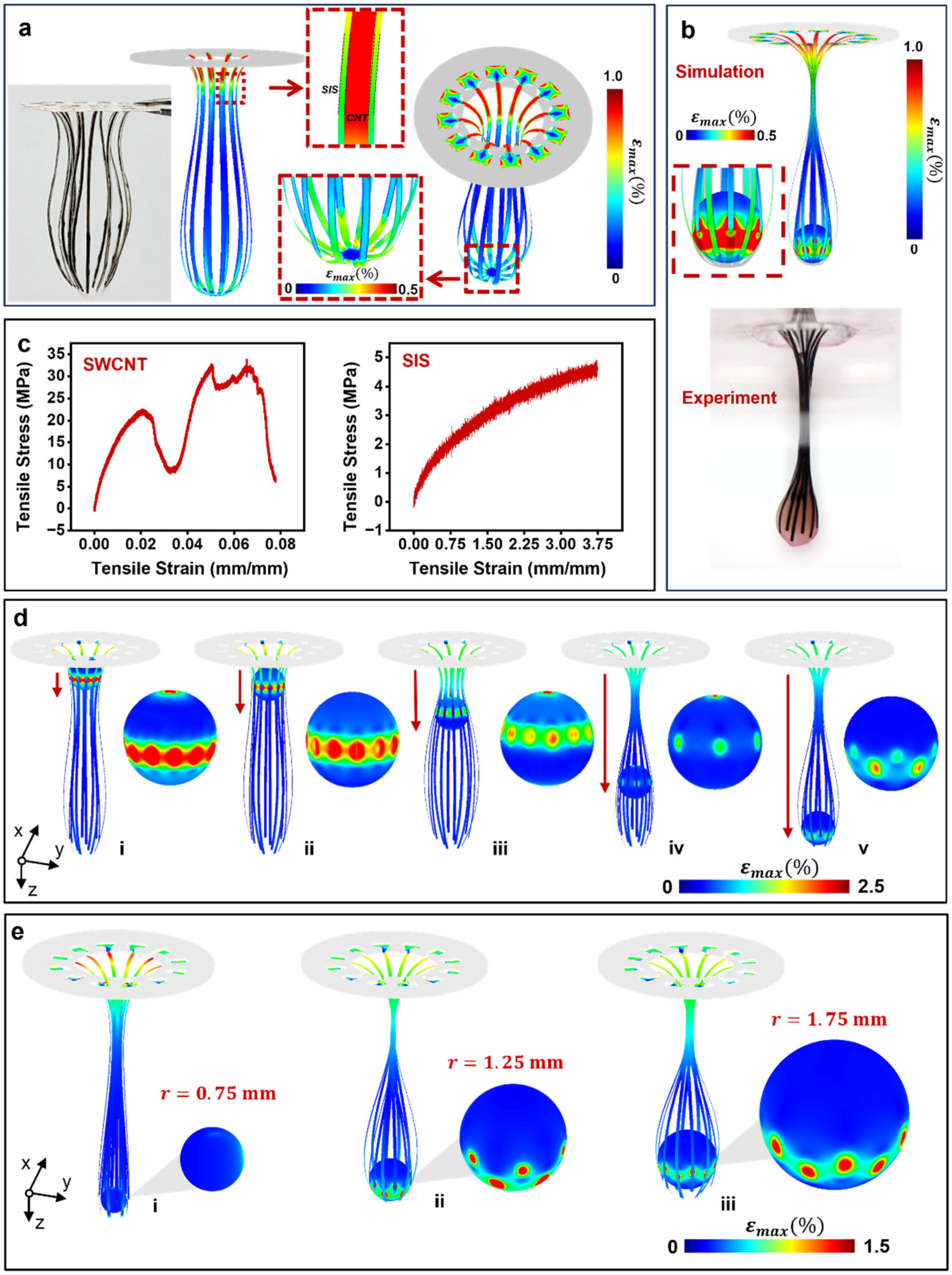

Figure S2: Mechanical modelling and characterisation. a) Finite element analysis (FEA) of a free-standing CAMEO, shown in top and side views. b) FEA of the CAMEO following organoid insertion, with a representative experimental image for comparison. c) Stress–strain responses of the SWCNT and SIS films used in the device. d) FEA simulations of the CAMEO mechanical response during organoid deposition and subsequent transport through the CAMEO legs. e) FEA simulations showing CAMEO deformation for representative organoid radii of 0.75 mm, 1.25 mm, and 1.75 mm.

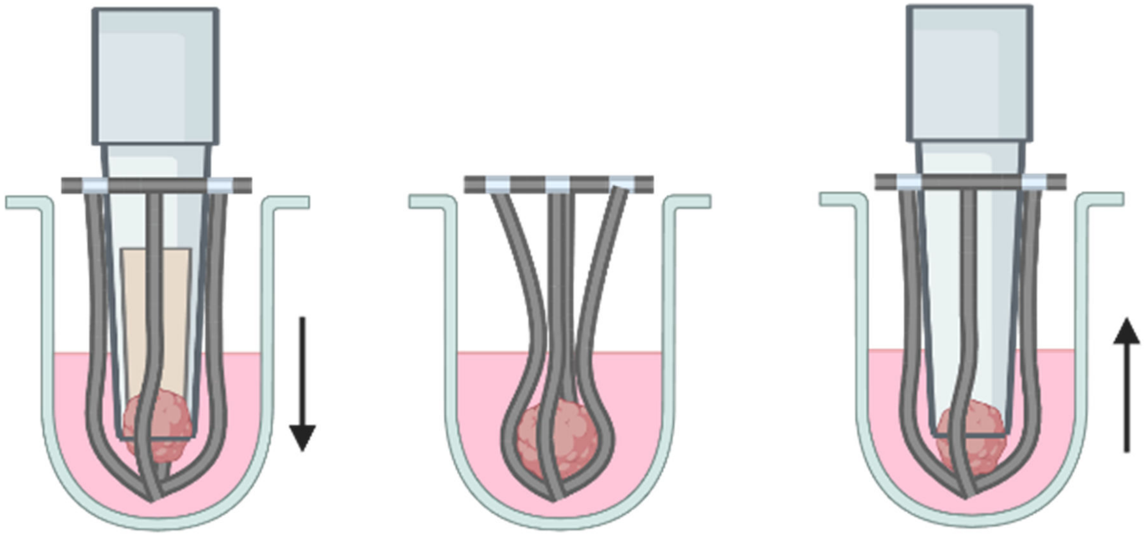

Figure S3: Schematic illustrating reversible insertion and removal of an organoid from a CAMEO. A wide cut pipette tip is introduced from the top to gently spread the compliant CAMEO legs, enabling placement or withdrawal of the organoid while the device is submerged in culture medium. Upon removal of the pipette tip, the flexible CAMEO legs relax and conform around the organoid, establishing a stable yet non-adhesive electrode-tissue interface. Created in BioRender. Mishra, N. (2026) https://BioRender.com/gqzc1xf.

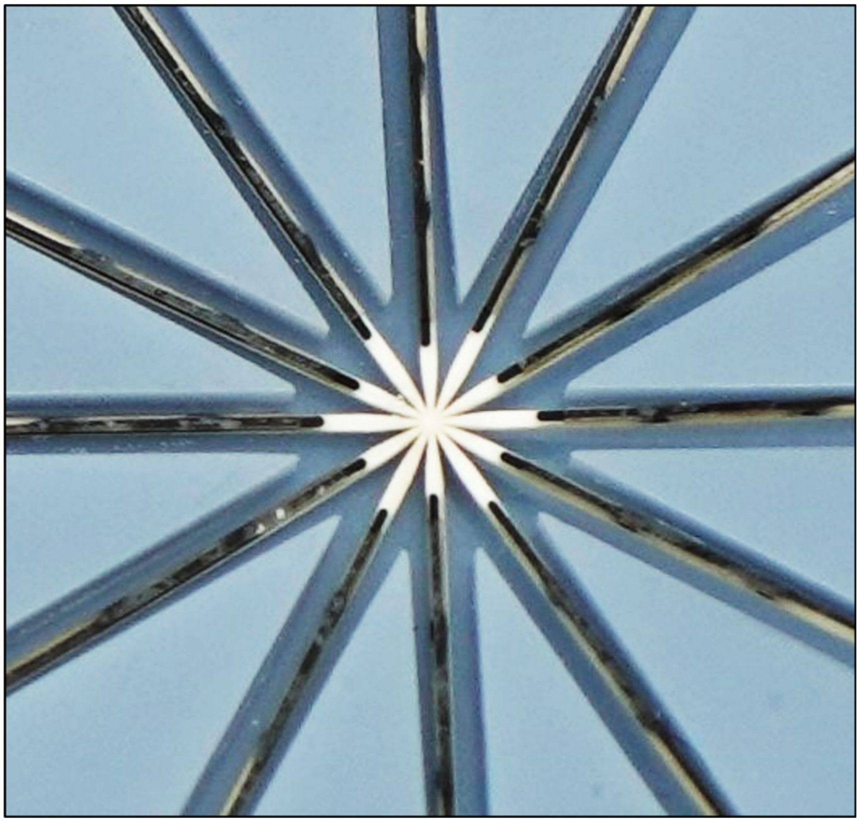

Figure S4: A close-up view of a cartwheel inside a trench.

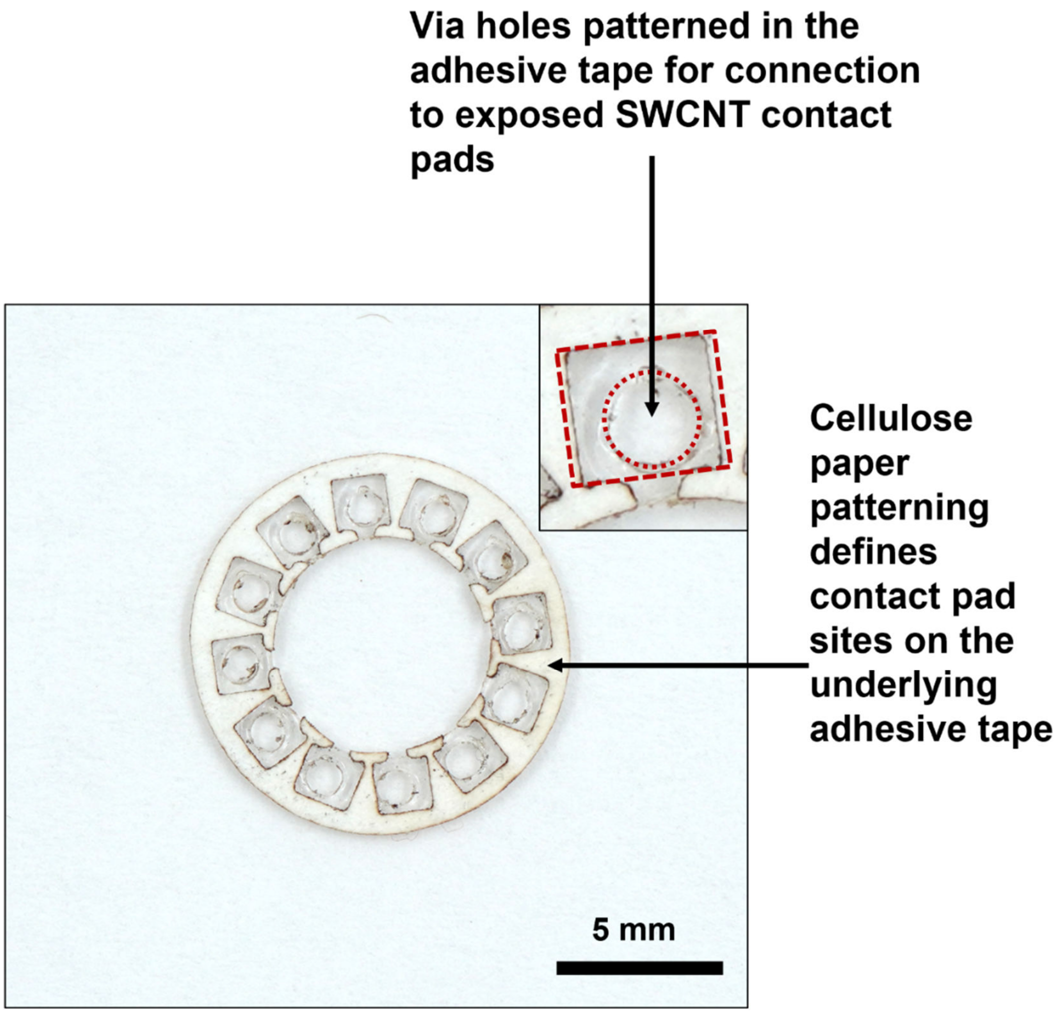

Figure S5: A close-up view of the assembly ring. Adhesive slots hold contact pads in place and patterned vias allow for electrical connection.

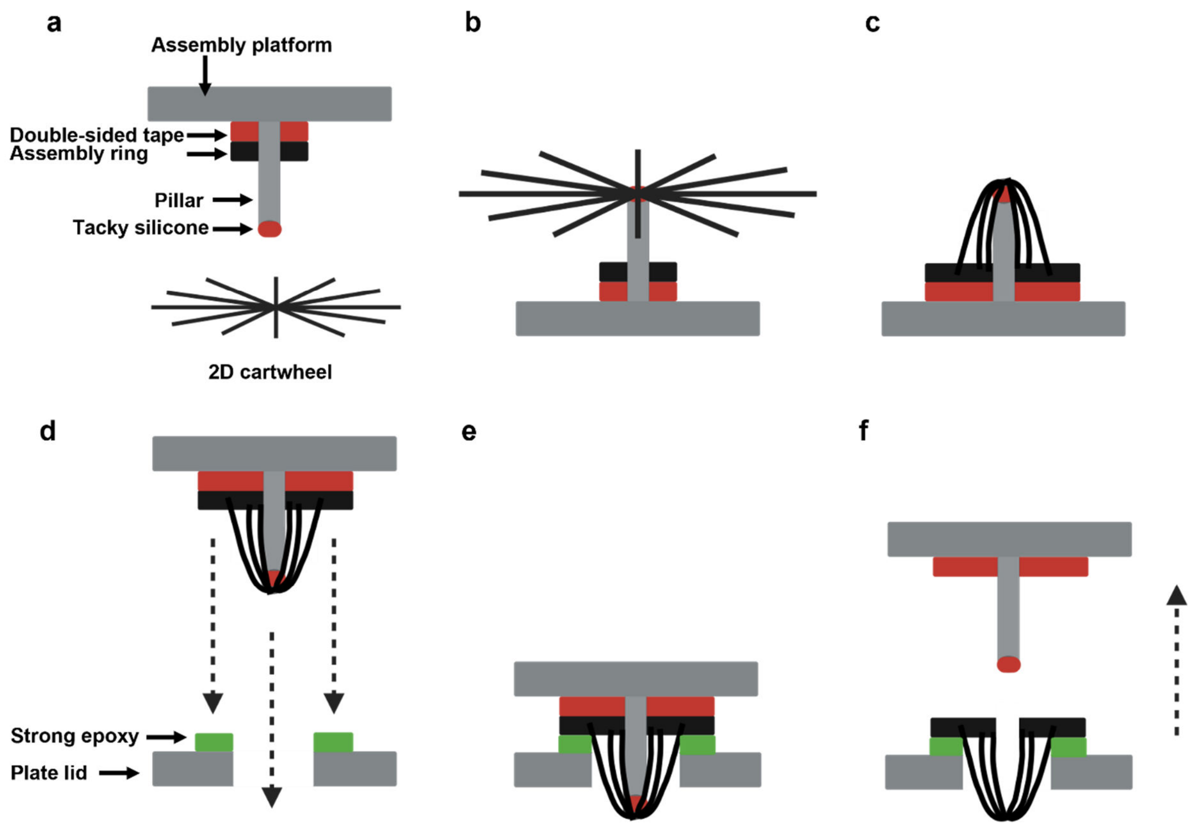

Figure S6: Schematic illustrating the adhesion-guided transfer of CAMEO devices from the assembly platform to the culture plate lid. a) The assembly platform consists of a 3D-printed stand with vertical pillars and an assembly ring positioned around the base of each pillar. Temporary adhesion is provided by a thin layer of tacky silicone applied to the pillar tip and a thin piece of double-sided tape applied to the pillar base. **b)** Upon inversion of the platform, the tacky silicone at the pillar tip makes contact with the planar 2D cartwheel and lifts it from the substrate via reversible adhesion. **c)** While the cartwheel centre and assembly ring are held in place by the silicone, the spokes bend and transform into the three-dimensional CAMEO geometry. **d)** The fully assembled CAMEO, still supported by the pillar, is inverted and inserted through a laser-patterned opening in the culture plate lid, where a ring of epoxy has been pre-applied. Dotted arrows show direction of assembly platform movement. **e)** Contact between the assembly ring and the epoxy results in permanent bonding of the CAMEO to the plate lid. **f)** Following epoxy curing, the assembly platform is lifted away; the weaker silicone adhesion releases cleanly from the pillar, leaving the CAMEO securely bonded to the culture plate. Dotted arrow shows direction of assembly platform movement. Created in BioRender. Mishra, N. (2026) https://BioRender.com/x6gd95x.

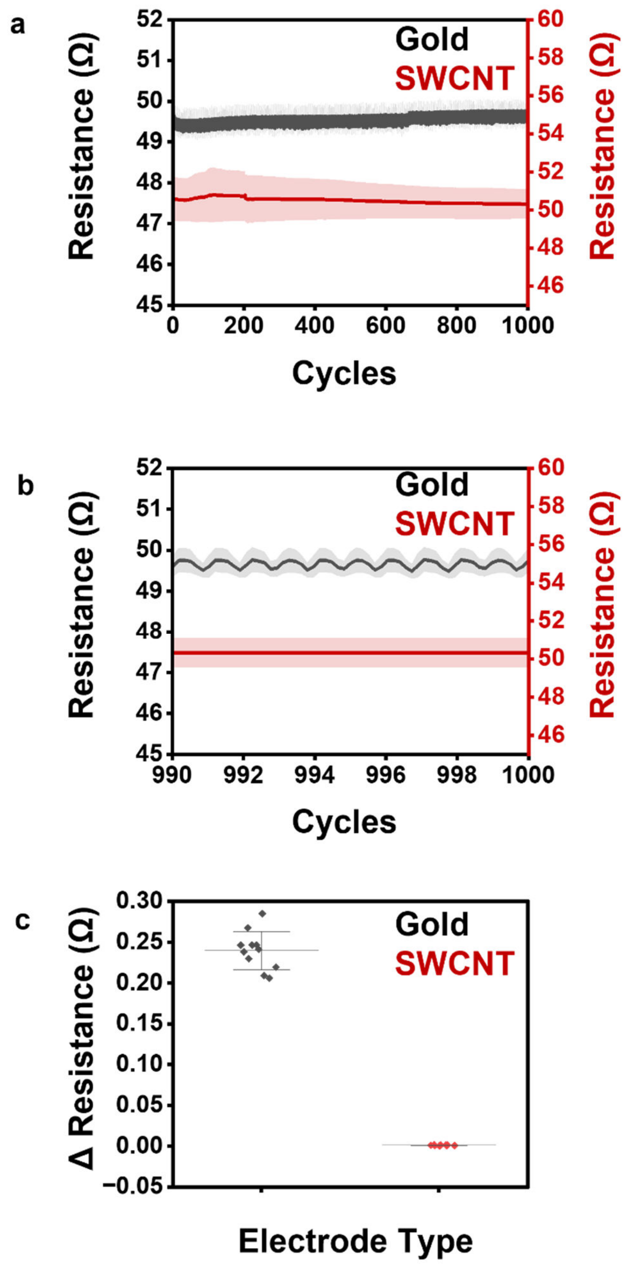

Figure S7: Electro-mechanical characterisation of SWCNT/SIS and Au/PI films. a) Evolution of resistance of Au and SWCNT electrodes over 1000 bending cycles. **b)** Resistance of Au and SWCNT electrodes during the last 10 bending cycles. **c)** Intra-cycle resistance change averaged over 10 bending cycles shows negligible change for SWCNT traces, whereas Au traces exhibit ~209-fold higher resistance change upon deformation. Data are presented as mean ± SD.

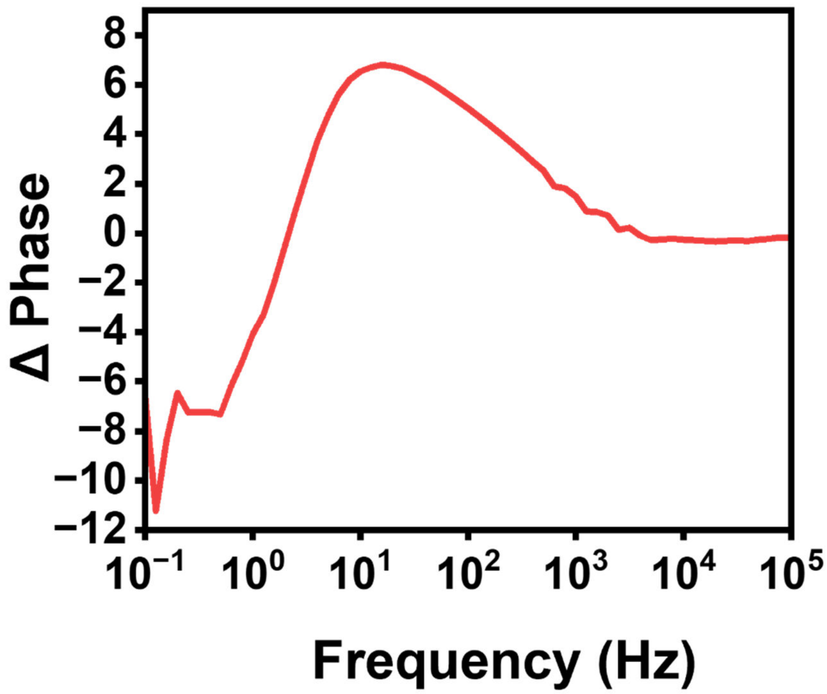

Figure S8. Electrochemical impedance spectroscopy (EIS)-based microcrack analysis. Phase difference (ΔPhase) between the 2D cartwheel and 3D CAMEO devices is plotted as a function of frequency, highlighting strain-induced microcrack formation within the SWCNT film. The frequency-localized response captures defect evolution during the 2D to 3D transformation, while the negligible shifts at spike-relevant frequencies (10^3 to 10^5 Hz range) confirm potential for unaltered recording performance.

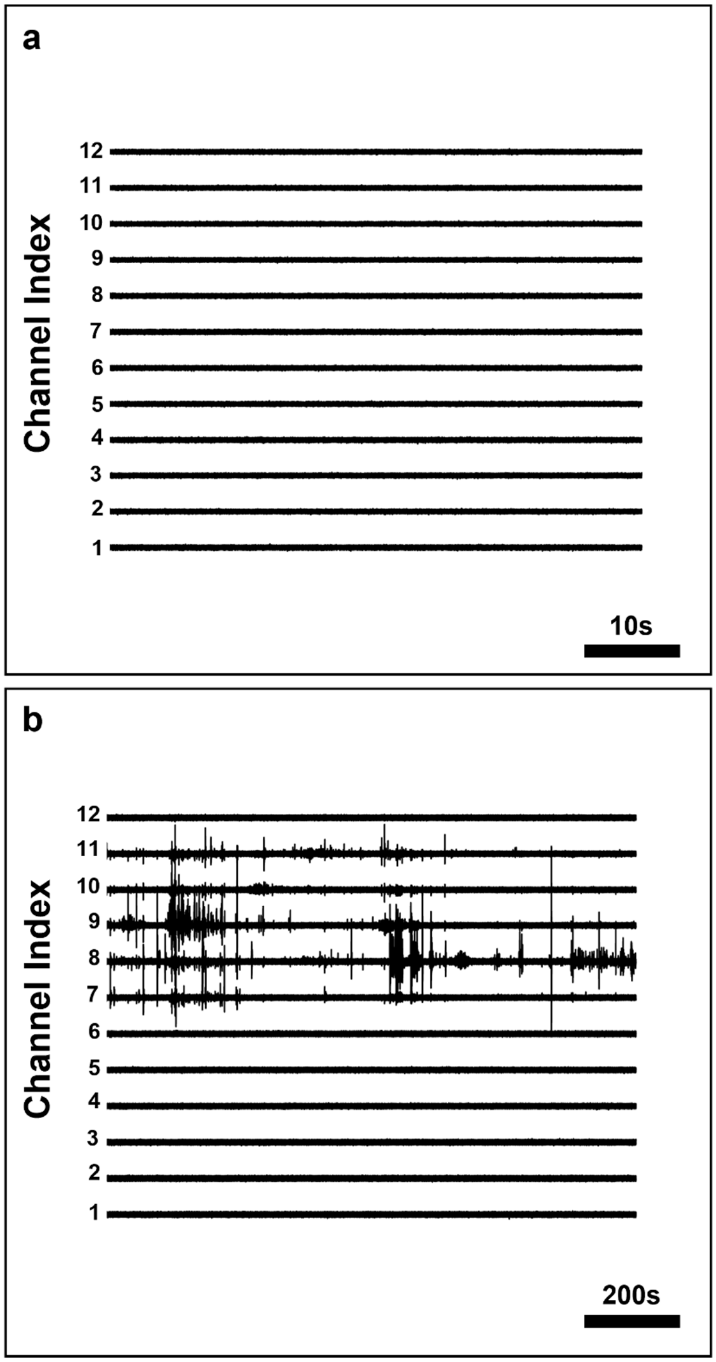

Figure S9: Electrophysiological recordings from a CAMEO before and after the insertion of an organoid into it. a) Control recording in media without an organoid in the CAMEO. **b)** Recording captured by CAMEO after placing an organoid in it.

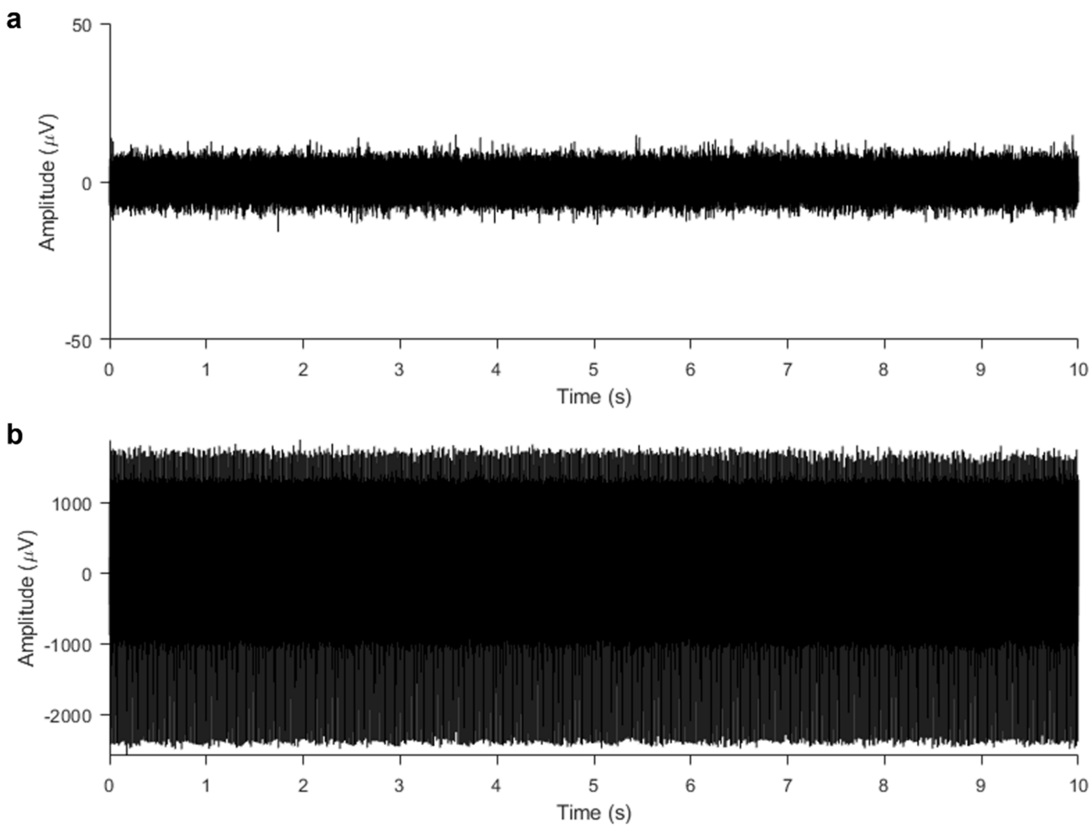

Figure S10. Representative voltage-time traces to distinguish biologically quiescent channels from electrically disconnected channels. **(a)** An electrically connected CAMEO channel exhibiting a stable, low-noise baseline. **(b)** An open-circuit channel characterised by markedly elevated noise levels.

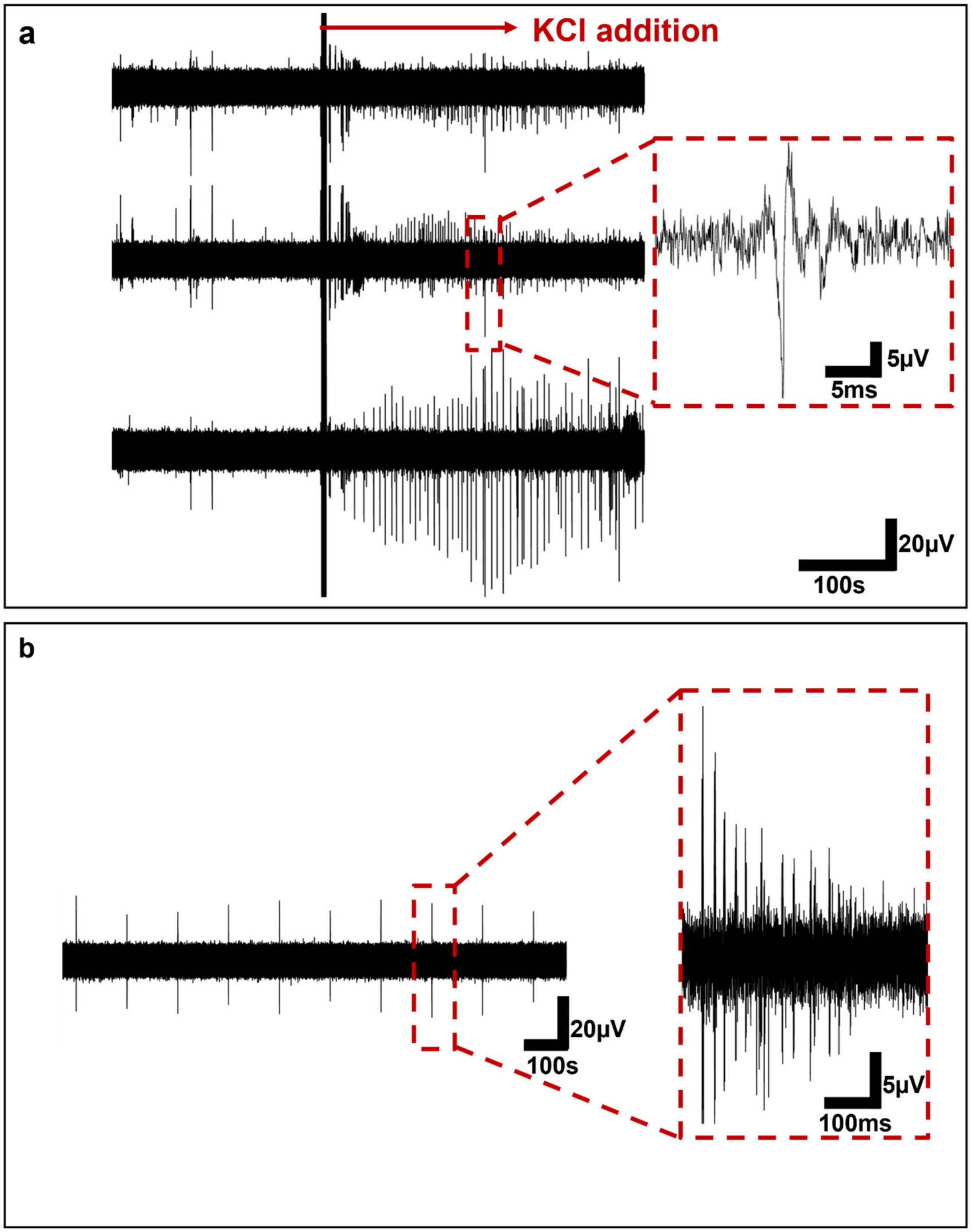

Figure S11: Electrophysiological activity of organoids. a) Pharmacological stimulation with KCl induces a marked increase in neural activity across three electrodes. **b)** Representative burst patterns recorded from organoids.

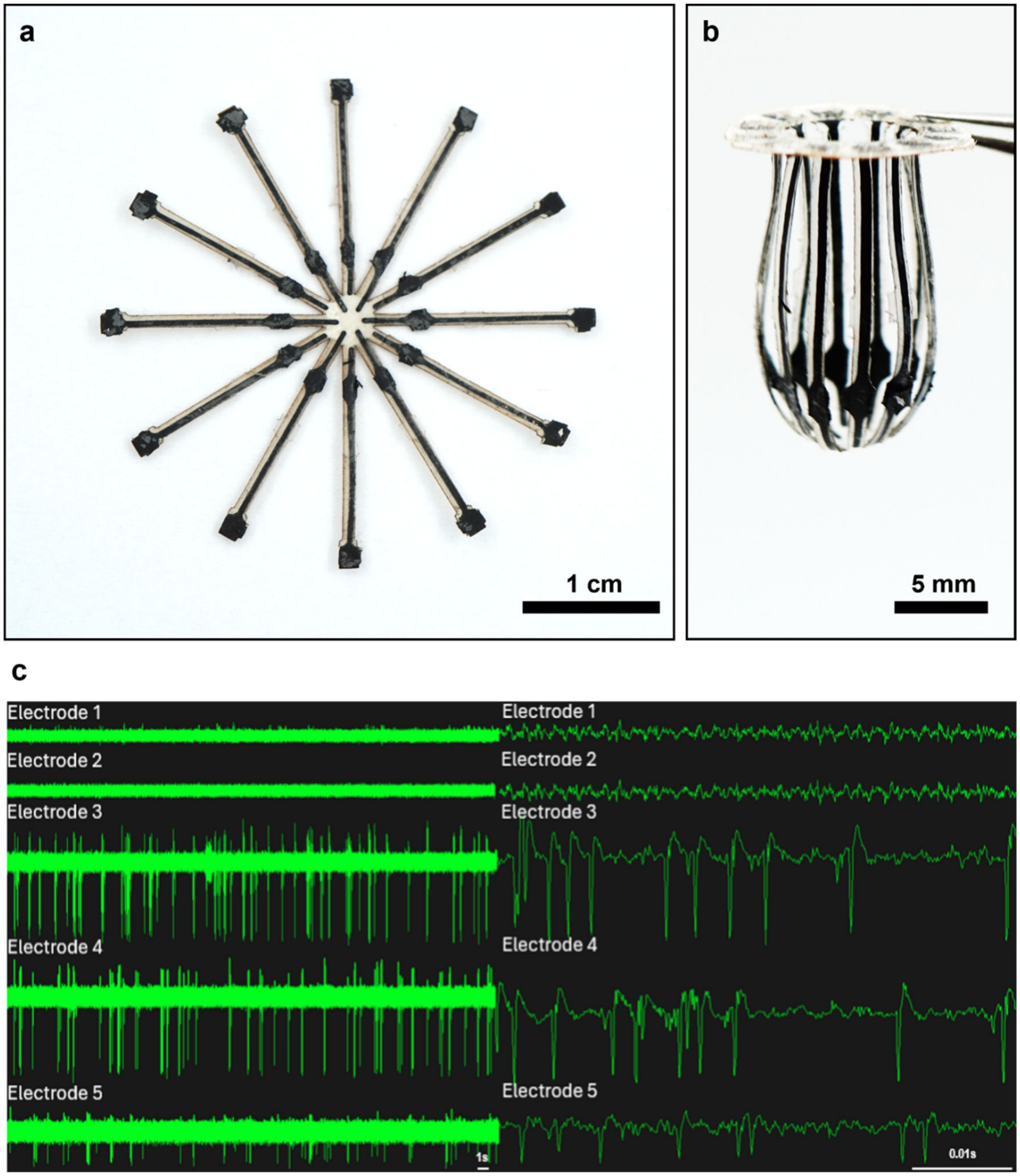

Figure S12: Low-resource alternatives for CAMEO fabrication and recording. a) A 12-spoke cartwheel fabricated using a low-cost CO_2 laser. **b)** Transformation of the CO_2 laser patterned cartwheel into CAMEO. **c)** Neural signal traces from an organoid in a CAMEO recorded using a low-cost bioamplifier (Neuron SpikerBox, Backyard Brains, Ann Arbor, MI) (left). The zoomed-in view of the traces shows distinct spike waveforms (right).

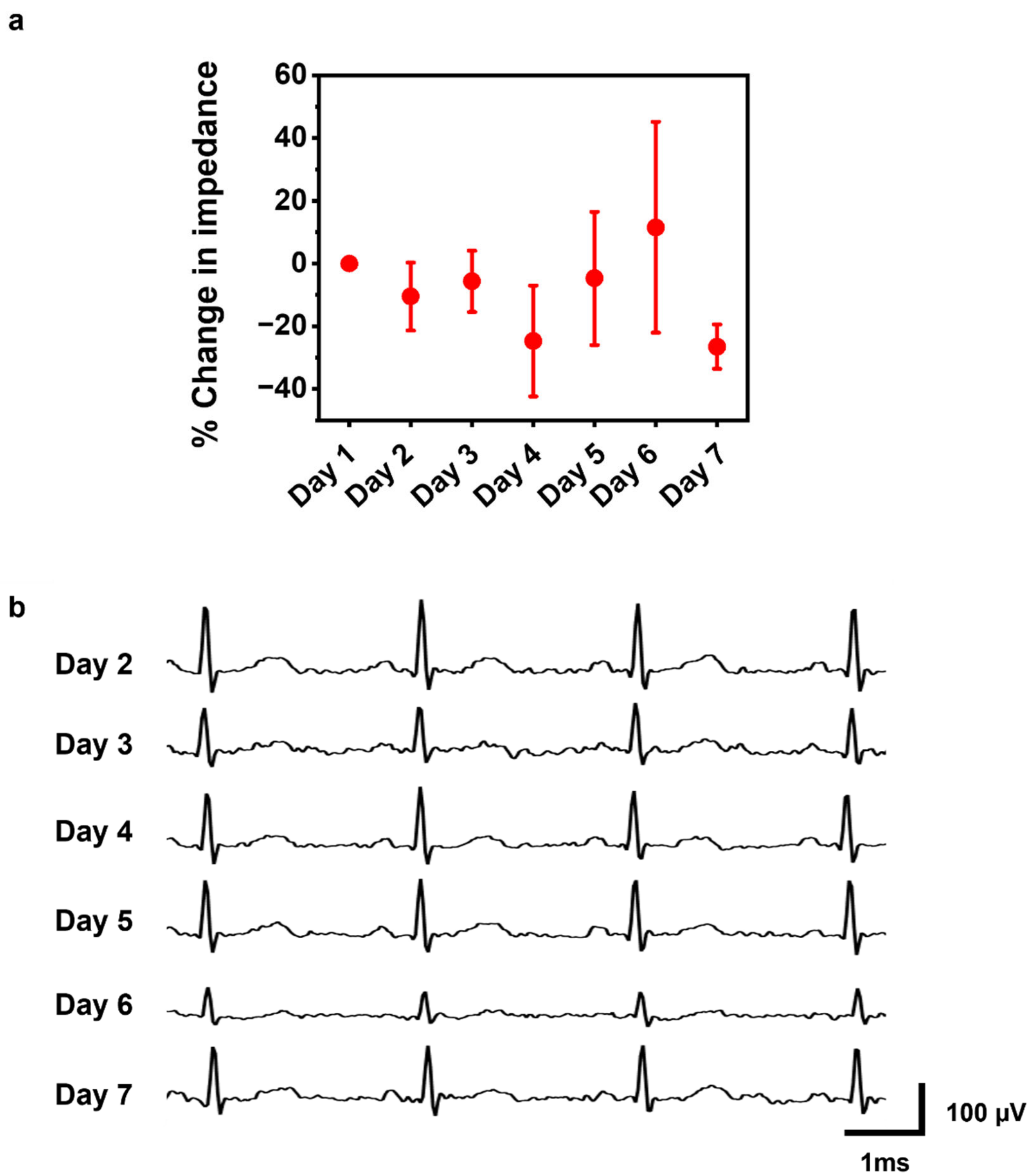

Figure S13: Accelerated aging assessment of CAMEO. a) Percent change in impedance at 1 kHz for n = 3 CAMEO electrodes during 7 days of incubation in phosphate-buffered saline at 60 °C, shows a maximum absolute deviation of ~26% relative to Day 1. All data are presented as mean ± SD. **b)** Representative voltage traces recorded from CAMEO in phosphate-buffered saline during application of an externally generated cardiac-like waveform across days 2-7, demonstrating continued electrical functionality and absence of catastrophic device failure throughout the accelerated aging period.

Table ST1: Density and Thickness Parameters Used for the Composite CAMEO Legs

	Density (ρ_i)	**Thickness (t_i)**	$\boldsymbol{\rho_i t_i}$
Top SIS	0.93 g/cm^3	0.002 cm	0.00186 g/cm^2
SWCNT	1.3 – 2.1 g/cm^3	0.001 cm	0.0013-0.0021 g/cm^2
Bottom SIS	0.93 g/cm^3	0.002 cm	0.00186 g/cm^2